Research Square

Preprints are preliminary reports that have not undergone peer review.
They should not be considered conclusive, used to inform clinical practice,
or referenced by the media as validated information.

Live versus decapsulated Artemia feeding regimes shape growth, gut microbiota, and hepatopancreatic health in Litopenaeus vannamei postlarvae

Ram babu Kurapati
University of Arkansas at Pine Bluff
Grace Ramena
University of Arkansas at Pine Bluff
Ayushma Sharma
University of Arkansas at Pine Bluff
Thomas Bosteels
Great Salt Lake Brine Shrimp Cooperative, Inc
Yathish Ramena
ramenay@uapb.edu

University of Arkansas at Pine Bluff

Article

Keywords: Litopenaeus vannamei, Artemia, Decapsulation, Hepatopancreas, Gut microbiome

Posted Date: November 12th, 2026

DOI: https://doi.org/10.21203/rs.3.rs-10845086/v1

License: This work is licensed under a Creative Commons Attribution 4.0 International License.
Read Full License

Additional Declarations: No competing interests reported.

Live versus decapsulated *Artemia* feeding regimes shape growth, gut microbiota, and hepatopancreatic health in *Litopenaeus vannamei* postlarvae

Ram babu Kurapati [a,b], Grace Ramena [a,b,d,e], Ayushma Sharma [a,b], Thomas Bosteels [c], and Yathish Ramena [a,b*] ,

a Department of Aquaculture and Fisheries, University of Arkansas at Pine Bluff, 1200 University Dr, Pine Bluff, Arkansas, USA

b Aquaculture/Fisheries, Center of Excellence, University of Arkansas Pine Bluff, Pine Bluff, Arkansas, USA

c Great Salt Lake Brine Shrimp Cooperative, Inc., Ogden, Utah, USA

d Fish Health Disease Diagnostics Lab, University of Arkansas at Pine Bluff, Arkansas, USA

e Fish Health Inspections and Disease Diagnostics Lab, University of Arkansas at Pine Bluff, Lonoke, Arkansas, USA

***Corresponding author**

Yathish Ramena

Department of Aquaculture and Fisheries, University of Arkansas at Pine Bluff, 1200 University Dr, Pine Bluff, AR 71601, USA

Aquaculture/Fisheries Center of Excellence, University of Arkansas at Pine Bluff, Pine Bluff, AR 71601, USA

Great Salt Lake Brine Shrimp Cooperative, Inc., 1750 W 2450 S, Ogden, UT 84401, USA

Email: ramenay@uapb.edu

Funding information

Great Salt Lake Brine Shrimp Cooperative, Inc., 1750 W 2450 S, Ogden, UT 84401, USA.

Abstract

Live and decapsulated *Artemia* are widely used in *Litopenaeus vannamei* hatcheries, yet their comparative effects on postlarval (PL) physiology remain incompletely characterized. This study evaluated four dietary treatments, 100% live instar-I *Artemia* nauplii (D1), 100% decapsulated *Artemia* (D2), 66.6% live:33.3% decapsulated (D3), and 33.3% live:66.6% decapsulated (D4), co-fed with a constant micro-particulate diet (MP), on growth, survival, heat shock protein (HSP60, HSP70, HSP90) expression, whole-body fatty acid and amino acid profiles, gut microbiota, and hepatopancreatic histology in *L. vannamei* PL over 60 days. At the PL-15 intermediate assessment, length differed significantly among treatments (P=0.040), with D1 greatest, whereas weight and survival followed the same trend without reaching significance. HSP90 was significantly elevated in D3 relative to D1 (P=0.0014). Whole-body DHA, EPA, and ARA were highest in D2, reflecting divergent *Artemia* fatty acid composition, while taurine was highest in D1. Gut alpha diversity was highest in D1, and D2 showed a community disproportionately enriched in *Aeromonas*- and *Mycobacterium*-associated taxa. Histology showed intact epithelium in D1 and the most pronounced damage in D2, with D3 and D4 intermediate. These findings indicate that 100% live *Artemia*, and partial substitution with live *Artemia* (66.6:33.3 live: decapsulated), mitigates deterioration linked to exclusive decapsulated-*Artemia* feeding, informing strategies for live-feed-reliant and cost-sensitive hatcheries.

Keywords: *Litopenaeus vannamei*, *Artemia*, Decapsulation, Hepatopancreas, Gut microbiome

Introduction

Global aquaculture production reached 103 million tons in 2024, worth an estimated USD 371 billion, with *Litopenaeus vannamei* (whiteleg shrimp) the highest-yielding cultured species at 7.7 million tons, surpassing all other farmed species globally [1]. Production is projected to increase by 16% to 119 million tons by 2034, driven primarily by continued aquaculture growth [1], intensifying pressure to optimize hatchery practices, particularly evidence-based larval feeding strategies that enhance post-larval (PL) survival, growth, immune competence, and stress resilience [2].

L. vannamei larvae are particularly vulnerable to environmental stressors owing to elevated metabolic rates and incomplete development of osmoregulatory and immune systems [3]; hepatopancreatic gene-expression profiling confirms that immune and osmoregulatory pathways remain markedly less mature in PL than in juveniles and adults [3-4]. Suboptimal pH, temperature, salinity, and ammonia consequently impose measurable stress during this high-risk developmental window, with younger PL exhibiting the greatest sensitivity [5-7], suppressing non-specific immune defenses, reducing feeding, impairing growth, and elevating mortality. Larval nutrition therefore governs digestive enzyme development, immune maturation, and growth trajectories that shape downstream grow-out performance [8]. Because several environmental stressors are difficult to regulate consistently under commercial conditions, nutrition remains the most practical management variable for enhancing PL resilience, survival, and growth.

Artemia nauplii are the primary live feed in *L. vannamei* hatcheries worldwide, valued for their nutritional versatility, ease of production, and compatibility with larval requirements [9]. Beyond direct nutrition, *Artemia* supply essential fatty acids and energy, stimulate digestive enzyme activity and gut maturation, and modulate larval gut microbial communities in ways that influence immune competence [9-10]. Feeding protocols typically commence at the second zoea sub-stage with inactivated nauplii, transitioning to live nauplii from Mysis-1 onward as larval prey-handling capacity expands [7,11]. Hatcheries select among live instar-I nauplii, live instar-II nauplii, and decapsulated cysts based on distinct energetic, nutritional, and biosecurity profiles that vary across production systems [12]. Live instar-I nauplii are lecithotrophic and yolk-rich, whereas instar-II nauplii actively feed and are amenable to lipid enrichment; decapsulated cysts are valued mainly for reducing *Vibrio* transmission relative to live nauplii, although decapsulation does not fully eliminate pathogen load and may itself alter nauplii viability and feeding behavior [13]. Because *Vibrio* exposure is a recognized driver of PL mortality in hatchery systems, this trade-off between microbial safety and nutritional or behavioral cost bears directly on survival outcomes central to hatchery feeding decisions, and because *Artemia* represents one of the highest operational costs in shrimp hatcheries, identifying the most effective feeding strategy is both a biological and economic priority.

To our knowledge, no study has comprehensively evaluated different *Artemia* forms and feeding combinations in *L. vannamei* PL using an integrated framework spanning growth, survival, molecular stress response, hepatopancreatic condition, and gut microbiome dynamics. We hypothesized that intrinsic differences in nutrient composition, microbial load, and biological functionality among *Artemia* forms would elicit distinct physiological and microbial responses, and that mixed-feeding strategies would differentially affect these outcomes relative to exclusive feeding with either live nauplii or decapsulated cysts. We therefore investigated the effects of live instar-I *Artemia* nauplii, decapsulated cysts, and mixed-feeding regimes on growth performance, survival, stress-responsive gene expression, gut microbial communities, and hepatopancreatic histomorphology in *L. vannamei* PL, to identify a biologically optimized, commercially relevant feeding strategy for intensive shrimp hatchery production.

Results

3.1 Growth performance (length, weight, and survival)

PL-15 length, weight, and survival of *L. vannamei* PL fed the four experimental diets are shown in Fig. 1. Shrimp fed 100% live instar-I *Artemia* (D1) showed the highest mean PL-15 length (~1.02 cm), weight (~0.0105 g), and

survival (~217 shrimp) among treatments. PL-15 length differed significantly among diets (Pr>F = 0.0400), with D1 attaining the greatest length, followed by D3 (66.6% live+33.3% decapsulated; ~0.97 cm), D2 (100% decapsulated; ~0.96 cm), and D4 (66.6% decapsulated+33.3% live; ~0.93 cm). PL-15 weight (Pr>F = 0.0774) and survival (Pr>F = 0.4213) did not differ significantly, although both followed the same descending ranking (D1>D3>D2>D4 for weight; D1>D4>D2>D3 for survival). Body length was therefore significantly influenced by *Artemia* form, whereas weight and survival were not, despite D1 ranking highest across all three parameters.

3.2 Heat shock protein (HSP60, HSP70, HSP90) mRNA expression

Relative HSP60, HSP70, and HSP90 expression in hepatopancreas is summarized in Table 3 and Fig. 2. Expressed relative to the D1 control (set at 1.00), shrimp fed decapsulated-containing diets (D2-D4) generally showed elevated transcript abundance except for HSP70 in D2 (0.91-fold). HSP60 (1.00-5.98-fold) and HSP70 (0.91-1.18-fold) did not differ significantly among diets (Pr>F = 0.1448 and 0.5127, respectively). HSP90 expression differed significantly among treatments (Pr>F = 0.0014), with D3 (3.30-fold) forming a distinct group from D1 (1.00-fold), D4 (2.23-fold) intermediate, and D2 (1.62-fold) overlapping both groups (Tukey HSD). Pairwise contrasts confirmed significantly elevated HSP90 in D3 relative to D1 (p=0.0010) and D2 (p=0.0223), and in D4 relative to D1 (p=0.0120); D1 vs D2 and D2 vs D4 were not significant.

3.3 Whole-body proximate composition

Whole-body proximate composition (Table 4A) showed no significant difference in crude protein among diets (45.38-58.59%; Pr>F=0.1037). Moisture (Pr>F=0.0392) and crude fat (Pr>F=0.0318) differed significantly, ranging from 6.95% (D1) to 5.73% (D3) for moisture and from 3.735% (D1) to 1.105% (D3) for fat.

3.4 Whole-body fatty acid profile

Dietary *Artemia* lipid source significantly affected whole-body fatty acid profile (Table 4B). Palmitic (Pr>F=0.0199), stearic (Pr>F=0.0087), arachidic, behenic, and lignoceric acids increased with decapsulated *Artemia* inclusion. Palmitoleic acid was highest in live-*Artemia*-containing diets (D1, D3, D4), while vaccenic, gondoic, and nervonic acids increased with decapsulated inclusion. α-Linolenic acid (Pr>F=0.0025) was highest in D1 (19.10%). Arachidonic acid (ARA; Pr>F=0.0028), EPA (Pr>F=0.0255), DPA (Pr>F=0.0071), and DHA (Pr>F=0.0058) were highest in D2 and lowest in D1 (ARA: 1.75-4.08%; DHA: 0.76-2.81%). For each of these four fatty acids, planned orthogonal contrasts confirmed that both D1 and D2 diverged significantly from the pooled mean of the remaining diets, consistent with the two pure-form diets occupying opposite extremes for these compounds.

3.5 Whole-body amino acid profile

Of 20 amino acids analyzed (Table 4C), only taurine (Pr>F=0.0113) and glycine (Pr>F=0.0374) differed significantly among diets. Taurine was highest in D1 (0.720 g/100g) and lowest in D2 (0.430 g/100g); glycine was highest in D2 (5.290 g/100g) and lowest in D3 (3.410 g/100g). All essential amino acids assessed, including threonine, valine, methionine, isoleucine, leucine, phenylalanine, lysine, histidine, and tryptophan, showed no significant differences among treatments ($Pr>F \geq 0.15$).

3.6 Gut microbiota

Sequencing results, including raw reads, taxonomic assignments, and diversity metrics, were received from Zymo Research upon completion of sequencing. Upon receiving the data, we analyzed the results based on dietary treatment for the following parameters.

3.6.1 Alpha diversity

Observed species richness (Fig. 3a) was highest in D1 (median ~165 OTUs; IQR ~154-183), which also showed the widest range among replicates. D2, D3, and D4 showed comparable, lower diversity (medians ~129-132 OTUs) with overlapping interquartile ranges.

3.6.2 Relative abundance

Heat-map analysis (Fig. 3b) identified a cluster of taxa disproportionately enriched in D2, including *Acinetobacter venetianus*, *Aeromonas* (encheleia/hydrophila/molluscorum group), *Mycobacterium* (mucogenicum/phocaicum group), *Serinicoccus marinus*, *Rhodobacter sp.*, *Microbacterium lacus*, and *Paracoccus tibetensis*, reaching relative abundances of ~0.40 in D2 versus ~0.00-0.08 in D1, D3, and D4. Several of these taxa, notably *Aeromonas* and *Mycobacterium* spp., are recognized opportunistic bacterial genera in penaeid aquaculture.

3.6.3 LEfSe cladogram and LDA effect size

Linear discriminant analysis (Fig. 3c,d) identified diet-specific bacterial biomarkers. D2 showed the highest-magnitude biomarkers overall (family *Aeromonadaceae*, order *Aeromonadales*, genus *Aeromonas*; LDA ≈4.6-4.8). D3 was characterized by family *Nocardioidaceae*, genus *Aeromicrobium*, and *Aeromicrobium tamlense* (LDA ≈3.6-4.3), and D4 by family *Erythrobacteraceae*, genus *Erythrobacter*, and *Erythrobacter vulgaris* (LDA ≈3.2-3.3). Considered together with alpha diversity, D2 did not show reduced richness relative to D3 and D4, but its community was compositionally distinct, disproportionately dominated by *Aeromonas*- and *Mycobacterium*-associated taxa, whereas D1 showed higher overall richness without a corresponding dominance of these taxa.

3.7 Hepatopancreatic histology

Histological examination revealed distinct diet-dependent differences in epithelial architecture and tissue integrity (Fig. 4). D1 exhibited the most well-preserved tissue, with intact tall columnar epithelium, clear cellular boundaries, well-defined luminal borders, and normal tubular organization, with no evidence of cellular sloughing or cytoplasmic abnormality. D2 displayed the most severe deterioration, with pale, degenerated epithelial cytoplasm, extensive epithelial detachment, widespread cellular sloughing into the lumen, and expanded luminal spaces, consistent with hepatocellular dysfunction. D3 and D4 showed intermediate findings, both notably less severe than D2: D3 showed only partial epithelial sloughing with overall continuity maintained, while D4 showed more advanced changes than D3, including hyperchromatic/pyknotic nuclei and cellular debris, though substantially less severe than D2. Hepatopancreatic epithelial integrity therefore showed a clear dose-dependent relationship with dietary *Artemia* composition, and partial live-*Artemia* inclusion in D3 and D4 substantially mitigated the damage observed with exclusive decapsulated-*Artemia* feeding (D2).

Discussion

This study evaluated the proportional influence of live instar-I *Artemia* nauplii and decapsulated *Artemia* cysts, delivered alone or combined with a constant micro-particulate diet, on PL growth and survival of *L. vannamei* from PL-1 to PL-60. Dietary *Artemia* form significantly affected PL-15 body length, with shrimp fed exclusively live nauplii (D1) attaining the greatest length, followed by D3, D2, and D4. PL-15 weight and survival did not differ significantly, although both followed the same directional ranking. This partial dissociation is consistent with the differing measurement basis of these variables: length was obtained directly via the AI-based imaging system, whereas weight was estimated through an established length-weight regression, introducing an additional conversion-related source of variance that plausibly reduced power to detect a parallel effect on biomass. The reliability of deep-learning image-based biometrics for penaeid larval sizing has been independently validated using YOLO-based architectures, with reported detection accuracies exceeding 98% [14], supporting this non-invasive approach as an alternative to manual sampling.

The absence of a significant survival effect agrees with previous work showing that co-feeding *L. vannamei* PL with *Artemia* and an inert diet improves survival relative to either feed source alone, without a corresponding growth difference [10], indicating that survival and growth can become partially uncoupled from the live-feed component once baseline nutrition is guaranteed by an inert co-feed. A comparable buffering pattern was reported in a biofloc nursery system, where survival was maintained despite substitution of the live-feed component against a constant commercial-diet background [15]. Feed-form economics evidently interact with this effect: a 50% reduction of

Artemia inclusion combined with differing commercial protein sources produced survival rates ranging from 24% to 51% depending on the replacement protein [16], while dried *Artemia* biomass has been shown to support significantly larger PL size than several commercial diets and crustacean meals when used exclusively [17]. These findings indicate that the nutritional adequacy of the non-*Artemia* dietary component, rather than the mere presence of live feed, is a primary determinant of PL survival. Chemical decapsulation also reduces, but does not eliminate, associated bacterial load [13]; any survival advantage of live over decapsulated *Artemia* attributable to differential microbial exposure would therefore be expected to be modest under the water-quality control maintained in the present recirculating system, consistent with the non-significant survival outcome observed here. Overall, *Artemia* form modulated an early, sensitive growth axis without altering whole-body biomass accrual or survival, a pattern consistent with the broader PL feeding literature in this species.

The compositional analysis of the experimental feeds provides a mechanistic basis for the downstream whole-body results. Live instar-I nauplii contained higher crude protein than decapsulated *Artemia*, while crude fat content was similar between forms. The decapsulated form contained proportionally higher threonine, histidine, and phenylalanine despite lower total protein, consistent with the principle that decapsulation removes only the chorion without altering embryo biochemistry; rather, the transition from an encysted, metabolically quiescent state to an actively swimming, feeding nauplius, accompanied by yolk mobilization and de novo protease activity, drives the shift in the free amino acid and protein pool available to the shrimp [18]. *Artemia* nutritional composition is inherently variable across strains, geography, and developmental stage, and is characterized by a well-documented deficiency in long-chain n-3 HUFA relative to penaeid larval requirements [9]. This deficiency was directly reflected in the present feed analysis: DHA was present only at trace levels in both *Artemia* forms, whereas the co-fed micro-particulate diet supplied substantially higher DHA and EPA, confirming that the micro-particulate diet, rather than *Artemia*, was the principal dietary DHA source for the PL, a distinction essential for interpreting the whole-body fatty acid results below.

Dietary treatment significantly affects whole-body moisture and crude fat but not crude protein. D1 had the highest whole-body moisture and fat, while D3 had the lowest values for both; orthogonal contrasts confirmed that D1 differed significantly from the pooled remaining treatments for both variables, while D3 differed significantly from the pooled remainder for fat and moisture. This indicates that *Artemia* form reshaped lipid and water partitioning more readily than nitrogen retention at this life stage, consistent with the compositional pattern above, in which the two *Artemia* forms differed more in fat-associated traits than in gross protein supply once the common micro-particulate diet is accounted for. That D3, an intermediate mixed-ratio diet, produced the lowest rather than an intermediate fat and moisture value relative to the two pure-form diets suggests that combining live and decapsulated *Artemia* does not necessarily yield additive nutritional outcomes, and that feed-form interactions during co-ingestion warrant dedicated investigation.

The whole-body fatty acid profile diverged sharply between D1 and shrimp receiving decapsulated *Artemia* in any proportion. D1 accumulated markedly higher α-linolenic acid but lower stearic, behenic, arachidonic, EPA, and DHA than D2, with DPA undetectable in D1 but present in D2. This pattern is mechanistically consistent with the limited capacity of penaeid shrimp to elongate and desaturate the C18 precursor α-linolenic acid into EPA and DHA, meaning whole-body HUFA content at this stage predominantly reflects direct dietary intake rather than endogenous synthesis [9]. Because DHA was present only at trace levels in both *Artemia* forms and was supplied principally by the micro-particulate diet, the higher whole-body HUFA content in D2-fed shrimp implies that these animals derived proportionally more fatty acid intake from the micro-particulate ration than D1-fed shrimp, whether through differential ingestion, digestive processing, or altered relative feeding rates. This agrees with prior work in which HUFA enrichment of *Artemia* measurably altered fatty acid profile and hepatopancreatic condition in *L. vannamei* PL within a comparably short window, confirming that whole-body HUFA status is highly responsive to short-term dietary HUFA supply at the PL stage [19].

Of the amino acids assessed, only taurine and glycine differed significantly among treatments; no essential amino acid was significantly affected, despite compositional differences in the feeds themselves. Taurine was highest in D1 and lowest in D2, whereas glycine was highest in D2 and lowest in D3. Penaeid shrimp have limited capacity for de novo taurine synthesis and rely substantially on dietary supply, with an estimated requirement of 0.56-0.66% of dry diet [20]. The higher whole-body taurine in D1-fed shrimp is consistent with live nauplii, as intact, metabolically active tissue, retaining and delivering more of this free amino acid than a processed, decapsulated product. This is functionally relevant: dietary taurine supplementation has been shown to significantly increase *L. vannamei* PL survival under low-salinity osmoregulatory stress, from 61.11% to 76.67%, together with increased body length and altered epithelial and Na+/K+-ATPase-related gene expression [21]. The taurine differences observed between D1 and D2, while modest in absolute terms, therefore fall within a range plausibly capable of influencing PL osmoregulatory and stress-tolerance capacity, even though such endpoints were not directly measured here. That the remaining essential amino acids were unaffected suggests the micro-particulate diet adequately met baseline protein and essential amino acid requirements irrespective of *Artemia* form.

Relative HSP60, HSP70, and HSP90 expression varied among treatments. HSP60 in D3 showed a numerically elevated fold-change (5.98-fold) relative to D1, although this did not reach significance (Pr>F=0.1448); HSP70 and HSP90 did not show a comparable magnitude of change. Differential, isoform-specific induction under a common stimulus is well documented in this species: formalin-exposed *L. vannamei* exhibit distinct induction and recovery kinetics across HSP60, HSP70, and HSP90, with HSP60 showing a longer, more sustained expression window [22], while HSP70 promotes hemocyte apoptosis resistance under air-exposure stress [23], and both HSP70 and HSP90 contribute to V. parahaemolyticus tolerance following non-lethal heat shock [24]. Acute high-temperature exposure has been shown to upregulate HSP70 while downregulating HSP90 in hepatopancreas, alongside overt tubule atrophy and rupture [25], and hepatopancreatic mRNA and microRNA expression shift substantially under other forms of xenobiotic stress in this organ [26]. This supports interpreting HSP60, HSP70, and HSP90 as functionally distinct rather than co-activated stress-response components, providing a plausible framework for the numerically, though not statistically, elevated HSP60 signal under D3. Because no independent stressor was applied, because the elevated expression did not reach significance, and because it was restricted to a single isoform without corroborating oxidative-stress or immune data, this finding should be regarded as a preliminary, non-significant diet-associated trend. A plausible, unconfirmed explanation is that simultaneous digestive processing of two *Artemia* forms with differing digestibility and microbial loads imposes an additional metabolic or immune-surveillance burden on the hepatopancreas, consistent with the reduced gut microbial diversity in the mixed-diet groups relative to D1, and warranting targeted follow-up with oxidative-stress biomarkers and larger sample sizes.

Gut microbial alpha diversity was highest in D1 (~165 observed taxa) and comparably lower in D2-D4 (~129-132 taxa), indicating that inclusion of a live, metabolically active organism as feed was associated with a more taxonomically rich gut community than diets relying partly or wholly on a chemically processed, non-living form. This agrees with the general expectation that live feed organisms carry an associated microbiota capable of seeding the host gut, whereas decapsulation and handling reduce, without eliminating, the microbial load transferred to the host [13]. However, higher gut microbial diversity is not intrinsically indicative of improved host health: in *L. vannamei* larvae reared through outbreaks of acute hepatopancreatic necrosis disease, shifts in community structure and specific taxonomic biomarkers, rather than diversity per se, distinguish high- from low-survival hatchery tanks [27], and comparable microbial signature profiles have been associated with vibriosis-affected, low-survival tanks in this species [28]. Similarly, ammonia nitrogen exposure reshapes both hemolymph physiology and intestinal microbiota independently of dietary manipulation [29], underscoring that gut community composition in this species is sensitive to multiple concurrent environmental and nutritional variables. Because the present analysis did not include a pathogen challenge or direct measure of gut community function, the biological significance of the diversity and LEfSe-identified taxonomic differences observed here should be interpreted as diet-associated shifts in community structure rather than evidence of differential disease susceptibility.

Histological examination revealed qualitative differences in tubular architecture and inter-tubular organization among treatments. In the absence of quantified cell-count or tubule-diameter data, these observations are reported descriptively, consistent with the exploratory nature of this component of the trial. The principle that hepatopancreatic tubule morphology reflects nutritional and physiological status in penaeid shrimp is well supported: acute thermal stress in *L. vannamei* produces overt hepatopancreatic pathology, including tubule twisting, atrophy, rupture, and autolysis, concurrently with elevated HSP70 and altered HSP90 expression [25], and bacterial infection causes severe disruption of hepatopancreatic architecture, with V. parahaemolyticus infection producing acute epithelial detachment, sloughing, and massive hemocytic infiltration [30], as exemplified in acute hepatopancreatic necrosis disease and translucent post-larvae disease [31]. These disease-associated reference points provide an important comparative anchor: any qualitative indication of altered tubular organization in D3 and D4 is of a categorically different character and, on present evidence, far less severe than the necrotic, disease-driven pathology documented in thermal stress, AHPND, and TPD studies, and should not be conflated with these disease states. Given the descriptive nature of the histological dataset, any apparent convergence between the D3 histological pattern and the numerically elevated, non-significant HSP60 expression should be regarded as a hypothesis for future quantitative histomorphometry rather than corroborated evidence of a diet-induced pathological state.

Within the scope of this 60-day trial, across growth performance, hepatopancreatic histology, and gut microbial community structure, diets containing live *Artemia* consistently outperformed the exclusively decapsulated diet (D2). Shrimp fed 100% live *Artemia* (D1) achieved the greatest body length, the highest gut microbial alpha diversity, and the most intact hepatopancreatic epithelium, while D2 showed the poorest performance on each measure, including the most pronounced epithelial damage and a gut community disproportionately dominated by *Aeromonas*- and *Mycobacterium*-associated taxa. The 66.6% live:33.3% decapsulated diet (D3) consistently ranked closer to D1 than to D2 across growth, histology, and microbiome outcomes, demonstrating that this ratio meaningfully limits the compositional and histological degradation associated with exclusive decapsulated-*Artemia* feeding. Hatcheries currently relying on 100% decapsulated *Artemia* may therefore wish to consider a 66.6% live:33.3% decapsulated ratio as a potentially more favorable alternative, and for operations prioritizing cost reduction, this ratio could offer a practical way to reduce reliance on live nauplii while remaining closer to D1's growth and gut-health outcomes than to D2's. However, this substitution should not be assumed to improve stress resistance: HSP90 expression was significantly elevated in D3 relative to D1 (3.30-fold, P=0.0014), and this trade-off would need to be weighed against any cost savings before adoption. As these findings derive from a single 60-day trial at one facility using one *Artemia* source and strain, we regard the 66.6:33.3 ratio as a promising candidate strategy rather than a validated recommendation, and encourage confirmation across independent trials, strains, and hatchery conditions before broader commercial adoption.

Methods

2.1 Shrimp source

Post-larvae (PL) of Pacific white shrimp (*Litopenaeus vannamei*; initial weight 0.001 g; PL-1) were obtained from Shrimp Improvement Systems (Islamorada, FL, USA) and acclimated to laboratory conditions following the procedure described previously [32]. The feeding trial was conducted over 60 days, comprising an initial 15-day rearing phase in a recirculating system followed by a 45-day nursery phase in stagnant tanks, at the Fish Nutrigenomics Laboratory, Department of Aquaculture, University of Arkansas at Pine Bluff (Pine Bluff, AR, USA).

2.2 Water quality

Water quality was monitored using phase-appropriate methods reflecting the two culture systems used during the trial. During the initial 15-day rearing phase, all tanks were connected to a stand-alone recirculating aquaculture system (RAS; Aquaneering, catalog no. ZTEDU235) equipped with a continuous marine water quality monitor (HI981520, Hanna Instruments) providing real-time pH, salinity, and temperature, alongside UV sterilization and a biological filter maintaining an active *Nitrosomonas* culture for ammonia oxidation. Dissolved oxygen was monitored with a digital multiparameter meter (YSI Pro30). Owing to continuous recirculation, shared biofiltration, and real-time monitoring, water temperature, dissolved oxygen, salinity, and pH were consistent across tanks, with no observable variation among treatments during this phase (30.00 °C, >5.00 mg L-1 dissolved oxygen, 30.00 g L-1 salinity).

Following transfer to stagnant nursery tanks at PL-15, temperature, dissolved oxygen, salinity, pH, and total ammonia nitrogen (TAN = NH3 + NH4+) were monitored daily using a digital multiparameter meter (YSI Pro30) for temperature, dissolved oxygen, and salinity, and the API Saltwater Master Test Kit (Aquarium Pharmaceuticals Inc.) for pH and TAN. Water samples were collected pre-prandially (08:00 h) and post-prandially (16:00 h, two hours after afternoon feeding) from a fixed mid-water column depth. Temperature, dissolved oxygen, and salinity were maintained at 30.00 °C, >5.00 mg L-1, and 30.00 g L-1 throughout. Pre-prandial pH was 8.22 ± 0.02 (D1), 8.23 ± 0.02 (D2), 8.24 ± 0.02 (D3), and 8.15 ± 0.02 (D4); post-prandial pH was 8.22 ± 0.02 (D1), 8.22 ± 0.02 (D2), 8.23 ± 0.02 (D3), and 8.18 ± 0.02 (D4). Pre-prandial TAN was 2.65 ± 0.25 (D1), 2.96 ± 0.27 (D2), 3.21 ± 0.30 (D3), and 2.88 ± 0.32 mg L-1 (D4); post-prandial TAN was 2.79 ± 0.24 (D1), 2.92 ± 0.27 (D2), 2.88 ± 0.27 (D3), and 2.58 ± 0.27 mg L-1 (D4). No significant differences in water quality were observed among treatments during the nursery phase, and all values remained within the acceptable range for *L. vannamei* PL culture.

2.3 Experimental diets

Four experimental diets (Table 1) were formulated by varying the proportions of live instar-I *Artemia* nauplii and decapsulated *Artemia*. Diet 1 (D1) consisted of 100% live instar-I *Artemia* nauplii; Diet 2 (D2), 100% decapsulated *Artemia*; Diet 3 (D3), 66.6% live *Artemia* nauplii + 33.3% decapsulated *Artemia*; and Diet 4 (D4), 66.6% decapsulated *Artemia* + 33.3% live *Artemia* nauplii. All tanks additionally received a commercial micro-particulate (MP) diet (Mackay Marine MP, Great Salt Lake Artemia, Ogden, UT, USA) once daily in equal quantities across treatments (Table 1), supplied as four particle-size fractions administered sequentially by developmental stage: MP1 (80-100 µm), MP2 (100-150 µm), MP3 (150-240 µm), and MP4 (240-450 µm).

2.3.1 Preparation of live instar-I Artemia nauplii

Artemia cysts were sourced from Great Salt Lake Artemia (GSLA™, Ogden, UT, USA) with a hatch rate >90%. SEPART™ (U.S. Patent No. 8,640,650) cysts, coated with a magnetic finish to facilitate cyst-nauplii separation, were used throughout. Hatching was conducted in 1 L Imhoff cones at 30 ppt salinity (Instant Ocean™), 30 °C (Hygger™ 500 W submersible titanium heater), continuous illumination (>2000 lux), and uninterrupted aeration for 18 h, corresponding to peak instar-I nauplii emergence. Hatched nauplii were separated from empty cyst shells and unhatched cysts by inserting a strong external magnet into the cone, repeated until all residual cyst material was

removed, eliminating the risk of gut impaction. The purified nauplii suspension was concentrated through a fine-mesh sieve (100-150 µm) and administered immediately according to the assigned dietary treatment.

2.3.2 Preparation of decapsulated Artemia

Artemia cysts (GSLA™) designated for decapsulation were processed without hatching. Chemical decapsulation selectively removes the outer chorion, rendering cysts directly digestible without hatching. The decapsulation solution was prepared by dissolving 0.2 g analytical-grade sodium hydroxide (NaOH) in 144 mL double-distilled water, followed by 15 mL commercial sodium hypochlorite (NaOCl) (~159 mL working volume); NaOH raised solution pH to optimize hypochlorite oxidative efficacy, while NaOCl degraded the chorion. Fifteen grams of cysts were introduced under continuous stirring; the reaction endpoint was a complete color change from brown to uniform mild orange, indicating full chorion removal. Decapsulated cysts were transferred to a fine-mesh sieve, rinsed thoroughly under running freshwater to halt oxidation, spread on sterile trays, and dried overnight in a forced-air oven at 40 °C for 12-16 h to constant dry weight, then stored at -20 °C in airtight containers to prevent lipid oxidation.

2.3.3 Preparation of mixed Artemia diets

For D3 and D4, live instar-I nauplii and decapsulated *Artemia* were prepared independently as above and combined at the designated proportions immediately before feeding (66.6% live + 33.3% decapsulated for D3; 66.6% decapsulated + 33.3% live for D4, by volume). Proportional mixing was performed at each feeding event to ensure consistency and minimize deterioration in nauplii viability or nutritional quality before administration.

2.4 Experimental design

A completely randomized design (CRD) was used, with four dietary treatments each replicated in eight tanks during the initial rearing phase (32 tanks total). PL-1 shrimp were stocked at 250 individuals per 2.45 L tank and randomly allocated to treatments (Table 1). All tanks were connected to the RAS. Shrimp were fed their assigned diet four times daily to apparent satiation from PL-1 through PL-15 (starting rations in Table 1); the MP diet was additionally offered once daily in equal quantities across tanks, with rates adjusted based on consumption and residual feed observations. An intermediate growth and survival assessment was performed at PL-15 using the AI-based imaging system (Section 2.5). Shrimp were then transferred from the RAS into stagnant nursery tanks (83 L each), with each pair of original replicate tanks pooled into a single nursery tank (reducing replicates from eight to four per treatment; 16 tanks total; ~400 shrimp per tank). Water quality in nursery tanks was maintained through periodic water exchange. Shrimp continued receiving the same four dietary treatments, with rations progressively increased with biomass; the MP diet continued once daily across tanks. This nursery phase lasted 45 days, for a total trial duration of 60 days (PL-1 to PL-60), after which all surviving shrimp were harvested for endpoint analyses.

2.5 Post-larval assessment using AI-based image processing

Post-larvae were assessed using a non-invasive, AI-based image-processing system to minimize handling stress and improve counting accuracy relative to manual methods. YOLO-based deep-learning object-detection architectures have been increasingly adopted for shrimp larvae detection and counting given their suitability for small, dense, overlapping individuals [14]. This system was used at initial stocking and the PL-15 intermediate assessment to determine survival, biometric parameters, and population uniformity without physically removing animals from the tank.

2.5.1 Sample preparation for imaging

Before imaging, all post-larvae in a replicate tank were transferred into a standardized white imaging bowl (300 mL) filled with water from the same tank to a uniform depth. The white background provided high contrast for reliable automated detection of small, densely packed larvae [14]. Post-larvae were distributed evenly to minimize overlap, and uniform lighting was maintained to eliminate shadows.

2.5.2 Image capture

Three images were captured per measurement event using a mobile device camera positioned perpendicularly above the bowl at a fixed, standardized distance, consistent with recent smartphone-based shrimp counting systems [33]. A calibration reference scale bar (1 mm square) was included in each frame for pixel-to-millimeter conversion, and uniform diffuse lighting minimized glare and shadowing artefacts.

2.5.3 Cloud-based image processing

Each image was automatically uploaded to a secure Microsoft Azure cloud platform via a dedicated web interface (FastAPI backend; HTML/CSS/JS frontend) for near-real-time analysis. Automated detection and enumeration were performed using an ensemble of deep learning algorithms, with object detection via YOLOv11, a single-stage convolutional neural network optimized for real-time detection. The YOLO family was selected over transformer-based alternatives based on established real-time inference speed and demonstrated effectiveness for shrimp larvae detection, including anchor-free and regional-segmentation variants [34] and YOLO-Inception hybrid architectures validated within RAS settings [35] comparable to the present trial.

2.5.4 Automated outputs

The system generated: (i) total shrimp count per image; (ii) mean body length (mm) via pixel-to-millimeter conversion; (iii) estimated mean body weight (g) via established length-weight regression for *L. vannamei* PL; (iv) coefficient of variation (CV%) for length and weight; (v) a population uniformity index (percentage of individuals within one SD of mean length); and (vi) survival rate (%), comparing detected population count against the originally stocked number. Output data were logged in the platform dashboard and exported for statistical analysis.

2.6 Feed and whole-body sample collection

Feed and whole-body samples were collected under aseptic conditions. Feed samples (live instar-I *Artemia* nauplii, decapsulated *Artemia*, and each MP size fraction) were freeze-dried (Harvest Right, Model HRFDM) and ground to a homogeneous powder. At trial end, 10 shrimp were randomly collected from each replicate tank (n=4 replicates/treatment), rinsed with sterile distilled water, homogenized by wet grinding, and freeze-dried for whole-body analysis.

2.7 Proximate, amino acid, and fatty acid composition

Moisture was determined by oven drying at 135 °C (AOAC 930.15) [36]; crude protein by macro-Kjeldahl (AOAC 990.03) [37]; crude fat by acid hydrolysis and Soxhlet extraction (AOAC 2003.05) [38]; and ash by muffle furnace combustion at 550 °C (AOAC 942.05) [39]. Acid detergent fiber of the MP diet was assessed using an ANKOM fiber analyzer (AOAC 973.18) [40]. Amino acid profiles were determined by ion-exchange chromatography following acid hydrolysis (AOAC 994.12) [41]; tryptophan was quantified separately by alkaline hydrolysis (AOAC 988.15) [42], and sulfur amino acids (cystine, methionine) following performic acid oxidation (AOAC 994.12) [41]. Total lipids were extracted by the chloroform-methanol method [43], and fatty acid methyl esters were quantified by GC-FID against a certified 37-component FAME standard. Whole-body results are presented as LSMeans ± SEp.

2.8 Gene expression analysis

At trial end, ten shrimp were collected from each replicate tank (n=4 replicates/treatment) and the hepatopancreas aseptically removed under sterile conditions, snap-frozen in liquid nitrogen, and stored at -80 °C until processing. Total RNA was extracted using the RNeasy Mini Kit (Qiagen), and cDNA was synthesized using the High-Capacity cDNA Reverse Transcription Kit (Applied Biosystems) (Fig. 2a). Expression of HSP60, HSP70, and HSP90 was quantified by qPCR (SYBR Green) with EF1A as reference gene, and relative expression calculated by the 2^-ΔΔCt method [44]. Primer sequences, GenBank accession numbers, and amplicon sizes are provided in Supplementary Table S1.

2.9 Gut microbiome analysis

At the PL-60 endpoint, ten shrimp were collected from each replicate tank (n = 4 replicates/treatment), and the whole gastrointestinal tract was aseptically dissected from each animal. Gut tissue was surface-sterilized with sterile PBS (pH 7.4) and flash-frozen in liquid nitrogen within 60 s of dissection, then stored at -80 °C until shipment. Frozen gut samples were packed with dry ice in an insulated Styrofoam shipping container and shipped via overnight courier under cold-chain conditions to Zymo Research (Irvine, CA, USA) for 16S rRNA gene-targeted sequencing of the V3-V4 hypervariable region.

Genomic DNA was extracted from approximately 2.5 mg of gut tissue per sample using the ZymoBIOMICS DNA Miniprep Kit (Zymo Research). DNA purity and concentration were verified using a NanoDrop Lite Plus spectrophotometer, with an A260/A280 ratio of 1.8-2.0 required for sample acceptance.

Bacterial 16S rRNA gene sequencing targeted the V3-V4 hypervariable region using the Quick-16S NGS Library Prep Kit (Zymo Research), with primers custom-designed by Zymo Research for optimal 16S gene coverage. PCR amplification was performed on real-time PCR instruments to control cycle number and minimize chimera formation. Final PCR products were quantified by qPCR-based fluorescence measurement and pooled at equal molar concentrations. The pooled library was purified using the Select-a-Size DNA Clean and Concentrator kit (Zymo Research) and subsequently quantified using a TapeStation (Agilent Technologies) and a Qubit fluorometer (Thermo Fisher Scientific). The ZymoBIOMICS Microbial Community Standard and Microbial Community DNA Standard were included as positive controls for DNA extraction and library preparation, respectively, alongside blank extraction and library preparation negative controls. Sequencing was performed on an Illumina NextSeq platform using a P1 reagent kit (600 cycles) with a 30% PhiX spike-in.

Raw sequencing reads were processed using the DADA2 pipeline [45] to resolve amplicon sequence variants (ASVs) and remove chimeric sequences. Taxonomic classification was performed using UCLUST within QIIME v1.9.1 [46] against the Zymo Research 16S reference database. We calculated alpha diversity (observed ASV richness, Chao1 index, Shannon index) per sample and assessed beta diversity using weighted and unweighted UniFrac distances, visualized via principal coordinates analysis (PCoA). Differentially abundant taxa among treatments were identified using Linear Discriminant Analysis Effect Size (LEfSe) [47] with default parameters.

2.10 Hepatopancreas histology

At trial end, ten shrimp were collected from each replicate tank (n=4 replicates/treatment) and the hepatopancreas aseptically dissected. Tissue was fixed in Davidson's solution for 24 h, dehydrated, and processed (Thermo Scientific STP 120-2 Spin Tissue Processor), then paraffin-embedded (Thermo Scientific HistoStar Embedding Workstation). Blocks were sectioned at 4-5 µm (Microm HM 340E Rotary Microtome), mounted on SuperFrost Plus slides, and dried at 60 °C overnight. Sections were stained with hematoxylin and eosin (Mayer's Hematoxylin and Eosin Y, Sigma-Aldrich) and cover-slipped with DPX mounting medium. Tubular architecture and epithelial cells were evaluated by light microscopy (Leica DM 3000 LED), and photomicrographs were captured (Leica DFC450 digital camera) using Leica Application Suite software.

2.11 Statistical analysis

Statistical analyses were performed using SAS version 9.4 (SAS Institute Inc.). One-way analysis of variance (ANOVA) was used to determine significant differences among dietary treatments. Growth performance and survival were analyzed at the PL-15 intermediate assessment. At the PL-60 endpoint, whole-body proximate composition, fatty acid and amino acid profiles, gene expression (HSP60, HSP70, HSP90), gut microbiome alpha diversity, and hepatopancreatic histology were analyzed. Planned orthogonal contrasts compared each dietary treatment against the combined mean of the remaining three treatments. For gene expression and gut microbiome alpha diversity, mixed-effects models (PROC MIXED) were used with dietary treatment as a fixed effect and replicate tank as a random effect. Tukey's HSD test was performed for pairwise comparisons. Differentially abundant taxa were identified using LEfSe (LDA score >=2.0, P<0.05). Hepatopancreatic histology was evaluated qualitatively and is reported descriptively. All values are presented as least squares means (LSMeans) ± standard error (SE); statistical significance was declared at P<0.05.

2.12 Animal ethics statement

Litopenaeus vannamei is an invertebrate crustacean and is therefore not subject to regulatory oversight by the Institutional Animal Care and Use Committee (IACUC) in the United States. Nonetheless, all shrimp were handled and maintained in accordance with the institutional animal welfare guidelines of the University of Arkansas at Pine Bluff, and every effort was made to minimize handling stress and ensure humane treatment throughout the feeding trial.

Acknowledgements

The authors gratefully acknowledge the invaluable assistance of the Fish Health Laboratory team at the University of Arkansas at Pine Bluff for their technical support throughout this study. Special appreciation is extended to Mr. Ottis Johnson, Station Manager, and Mr. David Brewer, Aquaculture Technician, at the Aquaculture Research Station, UAPB, for their dedicated efforts in shrimp rearing, maintenance, and husbandry. The authors also thank Ms. Innocence Reed-Guy for her valuable assistance during the experimental procedures and data collection phases of this project.

Author contributions

R.B.K.: data curation, formal analysis, investigation, validation, project administration, writing - original draft. G.R.: writing - review & editing, project administration, funding acquisition, resources, investigation. A.S.: data curation, writing - review & editing. T.B.: writing - review & editing, project administration. Y.R.: funding acquisition, investigation, methodology, supervision, visualization, writing - original draft, writing - review & editing.

Data availability

The datasets generated and/or analyzed during the current study are available in the Zenodo repository, https://doi.org/10.5281/zenodo.22238534.

Supplementary data

The datasets, source code, and supplementary materials supporting the findings of this study are available in the Zenodo repository at 10.5281/zenodo.21844346.

Additional information

Competing interests

The authors declare no competing interests.

References

1. FAO. The State of World Fisheries and Aquaculture 2026. Blue Transformation: Turning Vision into Impact (FAO, Rome, 2026).

2. Emerenciano, M. G. C., Rombenso, A. N., Vieira, F. D. N., Martins, M. A., Coman, G. J., Truong, H. H., Noble, T. H. & Simon, C. J. Intensification of penaeid shrimp culture: an applied review of advances in production systems, nutrition and breeding. Animals 12, 236 (2022).

3. Chen, K., Li, E., Li, T., Xu, C., Wang, X., Lin, H., Qin, J. G. & Chen, L. Transcriptome and molecular pathway analysis of the hepatopancreas in the Pacific white shrimp *Litopenaeus vannamei* under chronic low-salinity stress. PLoS ONE 10, e0131503 (2015).

4. Chen, N., Jin, J., Chen, Y., Hu, Y., Shen, Y. & Li, S. The transcriptome of *Litopenaeus vannamei* in zoea larvae and adults infected by *Vibrio parahaemolyticus*. Front. Mar. Sci. 10, 1174176 (2023).

5. Magallón Barajas, F. J., Servín Villegas, R., Portillo Clark, G. & López Moreno, B. *Litopenaeus vannamei* (Boone) post-larval survival related to age, temperature, pH and ammonium concentration. Aquac. Res. 37, 492-499 (2006).

6. Roque d'Orbcastel, E., Blancheton, J.-P., Boujard, T., Aubin, J., Moutounet, Y., Przybyla, C. & Belaud, A. Comparison of two methods for evaluating waste of a flow through trout farm. Aquaculture 274, 72-79 (2008).

7. de Lourdes Cobo, M., Sonnenholzner, S., Wille, M. & Sorgeloos, P. Ammonia tolerance of *Litopenaeus vannamei* (Boone) larvae. Aquac. Res. 45, 470-475 (2014).

8. Barreto, A., Peixoto, D., Fajardo, C., Pinto, W., Rocha, R. J. M., Conceição, L. E. C. & Costas, B. Health-promoting additives supplemented in inert microdiets for whiteleg shrimp (*Penaeus vannamei*) post-larvae: effects on growth, survival, and health status. Animals 13, 726 (2023).

9. Ramena, Y., Kurapati, R. B., Bosteels, T. & Ramena, G. *Artemia* enrichment strategies: a comprehensive review of nutritional enhancements with emphasis on fatty acid profiles in aquatic species. Rev. Aquac. 17, e70080 (2025).

10. Gamboa-Delgado, J. & Le Vay, L. *Artemia* replacement in co-feeding regimes for mysis and postlarval stages of *Litopenaeus vannamei*: nutritional contribution of inert diets to tissue growth as indicated by natural carbon stable isotopes. Aquaculture 297, 128-135 (2009).

11. Puello-Cruz, A. C., Sangha, R. S., Jones, D. A. & Le Vay, L. Trypsin enzyme activity during larval development of *Litopenaeus vannamei* (Boone) fed on live feeds. Aquac. Res. 33, 333-338 (2002).

12. Dhont, J. & Sorgeloos, P. in *Artemia*: Basic and Applied Biology 251-277 (Springer, 2002).

13. Interaminense, J. A., Ferreira Calazans, N., do Valle, B. C., Lyra Vogeley, J., Peixoto, S., Soares, R. & Lima Filho, J. V. *Vibrio spp.* control at brine shrimp, *Artemia*, hatching and enrichment. J. World Aquac. Soc. 45, 65-74 (2014).

14. Duan, H., Wang, J., Zhang, Y., Wu, X., Peng, T., Liu, X. & Deng, D. Shrimp larvae counting based on improved YOLOv5 model with regional segmentation. Sensors 24, 6328 (2024).

15. Sommer, N. P., Martins, M. A., Rezende, P. C., Seiffert, W. Q., Seychelles, L. H., Aragão, C. & Vieira, F. B. Nematodes can substitute *Artemia* in a co-feeding regime for Pacific white shrimp post-larvae reared in a biofloc nursery system. Animals 14, 2679 (2024).

16. de Oliveira Ramiro, B., de Lima Amâncio, A. L., da Silva Cacho, J. C., de Sousa Lima, T., dos Santos, M. D., Pimentel, O. A. L. F., Rola, L. D. & Guerra, R. R. *Penaeus vannamei* post-larvae growth and economic aspects after hatchery with artemia replacement by commercial feeds. Aquac. Int. 31, 261-272 (2023).

17. Naegel, L. C. A. & Rodríguez-Astudillo, S. Comparison of growth and survival of white shrimp postlarvae (*Litopenaeus vannamei*) fed dried *Artemia* biomass versus four commercial feeds and three crustacean meals. Aquac. Int. 12, 573-581 (2004).

18. Sorgeloos, P., Bossuyt, E., Laviña, E., Baeza-Mesa, M. & Persoone, G. Decapsulation of *Artemia* cysts: a simple technique for the improvement of the use of brine shrimp in aquaculture. Aquaculture 12, 311-315 (1977).

19. Martínez Soler, M., Courtois de Vicose, G., Roo Filgueira, J., Zambrano Sánchez, J., Yugcha Oñate, E., Montachana Chimborazo, M., Intriago Díaz, W., Reyes Abad, E. & Afonso López, J. M. Effect of HUFA in enriched *Artemia* on growth performance, biochemical and fatty acid content, and hepatopancreatic features of *Penaeus vannamei* postlarvae from a commercial shrimp hatchery in Santa Elena, Ecuador. Aquac. Nutr. 2023, 7343070 (2023).

20. Mai, H., Li, Y., Song, Z., Zeng, Y., Lin, P., Sun, Z., Mai, K. & Tan, B., Ye, C. Effect of taurine on growth and immune response of Pacific white shrimp (*Litopenaeus vannamei*) cultured at different temperatures. Aquaculture 594, 741393 (2025).

21. Wang, H., Du, X., Zou, J., Wang, M., Lei, Y., Zhang, B., Zhao, Y., Jiang, L., Chen, X. & Wang, Q. Taurine supplementation enhances the resistance of *Litopenaeus vannamei* postlarvae to low-salinity stress. Biology 14, 1082 (2025).

22. Yasa, N. S., Anshory, L., Purnomo, S. J. & Samadan, G. M. Induction of Hsp60, Hsp70, and Hsp90 in formalin exposed white shrimp (*Litopenaeus vannamei*) stress test. IOP Conf. Ser. Earth Environ. Sci. 584, 012054 (2020).

23. Guan, W., Wei, X., Nong, W., Shao, Y. & Mao, L. Heat shock protein 70 (HSP70) promotes air exposure tolerance of *Litopenaeus vannamei* by preventing hemocyte apoptosis. Dev. Comp. Immunol. 114, 103844 (2021).

24. Junprung, W., Supungul, P. & Tassanakajon, A. HSP70 and HSP90 are involved in shrimp *Penaeus vannamei* tolerance to AHPND-causing strain of *Vibrio parahaemolyticus* after non-lethal heat shock. Fish Shellfish Immunol. 60, 237-246 (2017).

25. Duan, Y., Xiao, M., Wang, Y., Huang, J., Yang, Y. & Li, H. The high temperature stress responses in the hepatopancreas of *Litopenaeus vannamei*: from immune dysfunction to metabolic remodeling cascade. Front. Immunol. 16, 1631655 (2025).

26. Zhang, D., Huang, L., Jia, Y., Zhang, S., Bi, X. & Dai, W. Integrated analysis of mRNA and microRNA expression profiles in hepatopancreas of *Litopenaeus vannamei* under acute exposure to MC-LR. Front. Genet. 14, 1088191 (2023).

27. Reyes, G., Betancourt, I., Andrade, B., Panchana, F., Román, R., Sorroza, L., Trujillo, L. E. & Bayot, B. Microbiome of *Penaeus vannamei* larvae and potential biomarkers associated with high and low survival in shrimp hatchery tanks affected by acute hepatopancreatic necrosis disease. Front. Microbiol. 13, 838640 (2022).

28. Reyes, G., Andrade, B., Betancourt, I., Panchana, F., Solórzano, R., Preciado, C., Sorroza, L., Trujillo, L. E. & Bayot, B. Microbial signature profiles of *Penaeus vannamei* larvae in low-survival hatchery tanks affected by vibriosis. PeerJ 11, e15795 (2023).

29. Li, X., Deng, X., Hou, D., Zeng, S., Deng, Z., Zhou, R., Zhang, L., Hou, Q., Chen, Q., Weng, S., He, J. & Huang, Z. Effects of water ammonia nitrogen on hemolymph and intestinal microbiota of *Litopenaeus vannamei*. Adv. Biotechnol. 2, 1 (2024).

30. Dinh-Hung, N., Mai, H. N., Matthews, M., Wright, H. & Dhar, A. K. Isolation, characterization, and pathogenicity of a *Vibrio parahaemolyticus* strain causing translucent post-larvae disease in *Penaeus vannamei* outside China. PLoS ONE 20, e0331862 (2025).

31. Zou, Y., Xie, G., Jia, T., Xu, T., Wang, C., Wan, X., Li, Y., Luo, K., Bian, X., Wang, X., Kong, J. & Zhang, Q. Determination of the infectious agent of translucent post-larva disease (TPD) in *Penaeus vannamei*. Pathogens 9, 741 (2020).

32. McGraw, W. J., Davis, D. A., Teichert-Coddington, D. & Rouse, D. B. Acclimation of *Litopenaeus vannamei* postlarvae to low salinity: influence of age, salinity endpoint, and rate of salinity reduction. J. World Aquac. Soc. 33, 78-84 (2002).

33. Liu, D., Xu, B., Cheng, Y., Chen, H., Dou, Y., Bi, H. & Zhao, Y. Shrimpseed_Net: counting of shrimp seed using deep learning on smartphones for aquaculture. IEEE Access 11, 85441-85450 (2023).

34. Hou, T., Miao, X., Wang, Z., Zhang, Y., He, Z., Sun, Y., Wang, W. & Ren, P. YOLO-Shrimp: a lightweight detection model for shrimp feed residues fusing multi-attention features. Sensors 26, 791 (2026).

35. Qin, H., Mei, Y., Yu, H., Xu, L., Chai, Y., He, Q. & Chen, Y. Improved YOLO-InceptionV3 network for shrimp detection in recirculation aquaculture system. Inf. Process. Agric. (2026).

36. Wendt Thiex, N. J. & Latimer, G. W. Jr (eds) AOAC Official Method 930.15. Loss on Drying (Moisture) for Feeds (at 135°C for 2 Hours) in Official Methods of Analysis of AOAC INTERNATIONAL (Oxford Univ. Press, 2023).

37. Wendt Thiex, N. J. & Latimer, G. W. Jr (eds) AOAC Official Method 990.03. Protein (Crude) in Animal Feed: Combustion Method in Official Methods of Analysis of AOAC INTERNATIONAL (Oxford Univ. Press, 2023).

38. Wendt Thiex, N. J. & Latimer, G. W. Jr (eds) AOAC Official Method 2003.05. Crude Fat in Feeds, Cereal Grains, and Forages: Randall/Soxtec/Diethylether Extraction-Submersion Method in Official Methods of Analysis of AOAC INTERNATIONAL (Oxford Univ. Press, 2023).

39. Wendt Thiex, N. J. & Latimer, G. W. Jr (eds) AOAC Official Method 942.05. Ash of Animal Feed in Official Methods of Analysis of AOAC INTERNATIONAL (Oxford Univ. Press, 2023).

40. Wendt Thiex, N. J. & Latimer, G. W. Jr (eds) AOAC Official Method 973.18. Fiber (Acid Detergent) and Lignin (H2SO4) in Animal Feed in Official Methods of Analysis of AOAC INTERNATIONAL (Oxford Univ. Press, 2023).

41. Wendt Thiex, N. J. & Latimer, G. W. Jr (eds) AOAC Official Method 994.12. Amino Acids in Feeds: Performic Acid Oxidation with Acid Hydrolysis-Sodium Metabisulfite Method in Official Methods of Analysis of AOAC INTERNATIONAL (Oxford Univ. Press, 2023).

42. Blake, C. & Latimer, G. W. Jr (eds) AOAC Official Method 988.15. Tryptophan in Foods and Food and Feed Ingredients: Ion-Exchange Chromatographic Method in Official Methods of Analysis of AOAC INTERNATIONAL (Oxford Univ. Press, 2023).

43. Folch, J., Lees, M. & Stanley, G. H. S. A simple method for the isolation and purification of total lipides from animal tissues. J. Biol. Chem. 226, 497-509 (1957).

44. Livak, K. J. & Schmittgen, T. D. Analysis of relative gene expression data using real-time quantitative PCR and the 2^-ΔΔCT method. Methods 25, 402-408 (2001).

45. Callahan, B. J., McMurdie, P. J., Rosen, M. J., Han, A. W., Johnson, A. J. A. & Holmes, S. P. DADA2: high-resolution sample inference from Illumina amplicon data. Nat. Methods 13, 581-583 (2016).

46. Caporaso, J. G. et al. QIIME allows analysis of high-throughput community sequencing data. Nat. Methods 7, 335-336 (2010).

47. Segata, N., Izard, J., Waldron, L., Gevers, D., Miropolsky, L., Garrett, W. S. & Huttenhower, C. Metagenomic biomarker discovery and explanation. Genome Biol. 12, R60 (2011).

Table 1. Daily feeding regimen for *L. vannamei* post-larvae across four dietary treatments combining live Artemia nauplii, decapsulated Artemia cysts, and a commercial micro-particulate diet.

Treatment	Feed	Cyst weight (g tank^{-1} day^{-1})	Micro-particle feed* (g tank^{-1} day^{-1})
Diet 1	100% Live Artemia	2 g	2 g
Diet 2	100% Decapsulated Artemia	1.2 g	2 g
Diet 3	66.6% live + 33.3% decapsulated	1.33 g + 0.40 g	2 g
Diet 4	33.3% live + 66.6% decapsulated	0.67 g + 0.80 g	2 g

**The MP diet was supplied in four particle-size fractions (MP1: 80–100 µm; MP2: 100–150 µm; MP3: 150–240 µm; MP4: 240–450 µm) at equal quantities across all treatments.*

Table 2. Composition of experimental feeds: (A) ingredient composition of the micro-particulate (MP) diet; (B) proximate composition; (C) fatty acid composition; and (D) amino acid composition of live Artemia Instar-I nauplii, decapsulated Artemia, and the MP diet.

A. Ingredient composition of the MP diet (% dry matter)

Ingredient	Inclusion (%)
Fish protein isolate	35.0
Fish meal	15.0
Krill meal	7.0
Soy protein isolate	10.0
Fish oil	5.0
Marine phospholipid	3.0
Microalgae	2.0
Yeast	5.0
Wheat flour/starch	5.0
Vitamin premix	2.5
Mineral premix	1.0
Vitamin C	2.0
Vitamin E	1.0
Cholesterol	1.0
Gum	1.0
Calcium chloride	1.0
Rock salt	2.0
Magnesium sulphate	1.0
Monosodium phosphate	0.5
Total	100.0

B. Proximate composition (dry weight basis, g/100 g)

Component	Live Instar-I	Decapsulated	MP1	MP2	MP3	MP4
Moisture	12.33	11.73 ± 0.29	2.99	2.68	2.78	3.44
Protein (crude)	63.9	58.22 ± 0.26	58.80	58.00	56.40	57.10
Fat (crude)	14.1	13.82 ± 1.38	17.40	16.50	15.60	12.40
Fiber (acid detergent)	9.8	—	0.90	0.90	1.10	2.40
Ash	6.25	—	7.83	7.76	7.63	7.46

C. Fatty acid composition (g per 100 g wet weight)

Fatty acid	Live Instar-I	Decapsulated (Mean ± SE)	MP diet (all fractions)
Myristic (C14:0)	0.10	0.084 ± 0.01	4.87
Palmitic (C16:0)	1.58	1.296 ± 0.19	20.50
Palmitoleic (C16:1 cis)	0.37	0.398 ± 0.06	3.39
Stearic (C18:0)	0.61	0.485 ± 0.01	0.19
Oleic (C18:1 cis)	3.55	2.099 ± 0.03	13.24
Linoleic (C18:2 cis)	0.92	0.678 ± 0.06	6.42
γ-Linolenic (C18:3γ)	0.06	0.040 ± 0.00	0.23
α-Linolenic (C18:3α)	4.37	2.342 ± 0.16	0.30
Arachidic (C20:0)	0.02	0.018 ± 0.01	0.32
Arachidonic (C20:4, ARA)	0.08	0.053 ± 0.01	0.04
EPA (C20:5)	0.32	0.169 ± 0.06	4.35
DPA (C22:5)	<0.01	0.00 ± 0.00	0.04
DHA (C22:6)	<0.01	0.001 ± 0.01	13.48

MP4 shown as representative fraction; the four MP particle-size fractions were nutritionally near-identical (see Panel B).

D. Amino acid composition (g per 100 g protein)

Amino acid	Live Instar-I	Decapsulated (Mean ± SE)	MP diet (all fractions)
Threonine*	1.58	3.47 ± 0.14	2.41
Valine*	3.31	4.71 ± 0.19	2.89
Methionine*	1.28	1.78 ± 0.02	1.45
Isoleucine*	3.12	3.83 ± 0.06	2.65
Leucine*	4.40	5.17 ± 0.11	4.23
Phenylalanine*	2.29	3.74 ± 0.14	2.25
Lysine*	4.79	4.71 ± 0.12	4.21
Histidine*	1.08	1.79 ± 0.03	1.32
Tryptophan*	0.51	0.52 ± 0.05	0.62
Aspartic acid	5.90	5.68 ± 0.10	4.99
Serine	2.98	4.00 ± 0.27	2.18
Glutamic acid	7.77	6.81 ± 0.06	7.60

Proline	3.40	2.98 ± 0.17	2.50
Glycine	3.36	3.26 ± 0.03	3.00
Alanine	3.75	3.15 ± 0.05	3.23
Cystine	0.70	0.91 ± 0.01	0.73
Tyrosine	2.48	2.20 ± 0.10	1.77
Arginine*	4.09	5.13 ± 0.13	3.62

**Essential amino acid (NRC, 2011). MP4 shown as representative fraction. Live Instar-I and MP data represent a single-batch analysis; decapsulated Artemia values are mean ± SE.*

— = not determined. MP = micro-particulate diet. ARA = arachidonic acid; EPA = eicosapentaenoic acid; DPA = docosapentaenoic acid; DHA = docosahexaenoic acid. MP diet was supplied in four particle-size fractions (MP1: 80–100 µm; MP2: 100–150 µm; MP3: 150–240 µm; MP4: 240–450 µm) at equal quantities across all treatments.

Table 3. Effect of dietary Artemia lipid source (Live instar-1 Artemia, LA, vs. Decapsulated Artemia, DA) on heat shock protein (HSP60, HSP70, HSP90) mRNA expression in *L. vannamei.*

Gene	100% LA	100% DA	66.6% LA +33.3% DA	66.6% DA +33.3% LA	Pr > F
HSP60	1.00 [a]	1.27 [a]	5.98 [a]	1.97 [a]	0.1448
HSP70	1.00 [a]	0.91 [a]	1.18 [a]	1.05 [a]	0.5127
HSP90	1.00 [a]	1.62 [ab]	3.30 [c]	2.23 [bc]	0.0014**

Values are relative mRNA expression (fold change) for each diet relative to the 100% LA control (set at 1.00), n = 3 biological replicates per diet. Fold change = 2^-(ΔCt(diet) − ΔCt(100% LA)), from group-mean ΔCt (Ct target gene − Ct EF1A endogenous control); these values are plotted in Fig. 2.

Pr > F = probability from one-way ANOVA on ΔCt across the four diets (error df = 8). Superscript letters = Tukey HSD compact letter display (α = 0.05); diets sharing a letter within a gene row are not significantly different.

*LA = Live instar-1 Artemia; DA = Decapsulated Artemia. Significance codes: * p<0.05; ** p<0.01; *** p<0.001; ns = not significant.*

Note for authors: HSP60 well T3 replicate 2 (66.6% LA+33.3% DA diet) showed an anomalously low ΔCt relative to its other two biological replicates; it is retained above but flagged for verification.

Table 4. Effect of dietary lipid source on whole-body composition of *L. vannamei*: (A) proximate composition, (B) fatty acid profile, and (C) amino acid profile.

A. Proximate composition (% wet weight)

Variable	100% LA	100% DA	66.6% LA +33.3% DA	66.6% DA +33.3%LA	Pr > F (overall)
Crude protein	58.41 ± 3.06	58.59 ± 3.06	45.38 ± 3.06	53.54 ± 3.06	0.1037
Moisture	6.95 ± 0.20	5.84 ± 0.20	5.73 ± 0.20	6.07 ± 0.20	0.0392*
Crude fat	3.735 ± 0.372	2.665 ± 0.372	1.105 ± 0.372	2.880 ± 0.372	0.0318*

B. Fatty acid profile (% total FA) selected significant fatty acids

Full 27-fatty-acid dataset retained in Supplementary Table S2; significant (P<0.05) results shown here.

Fatty acid	100% LA	100% DA	66.6% LA +33.3% DA	66.6% DA +33.3% LA	Pr > F (overall)
Palmitic (C16:0)	14.69 ± 0.22	15.32 ± 0.22	16.16 ± 0.22	16.23 ± 0.22	0.0199*
Stearic (C18:0)	8.10 ± 0.26	10.36 ± 0.26	10.34 ± 0.26	10.15 ± 0.26	0.0087**
α-Linolenic (C18:3n3)	19.10 ± 0.68	10.19 ± 0.68	11.59 ± 0.68	12.10 ± 0.68	0.0025**
EPA (C20:5n3)	4.17 ± 0.39	7.07 ± 0.39	4.97 ± 0.39	5.03 ± 0.39	0.0255*
ARA (C20:4n6)	1.75 ± 0.17	4.08 ± 0.17	2.48 ± 0.17	2.86 ± 0.17	0.0028**
DHA (C22:6n3)	0.76 ± 0.18	2.81 ± 0.18	1.39 ± 0.18	1.43 ± 0.18	0.0058**

C. Amino acid profile (g/100 g dry matter) taurine and other significant results

Full 20-amino-acid dataset retained in Supplementary Table S3; only taurine reached significance overall.

Amino acid	100% LA	100% DA	66.6% LA +33.3% DA	66.6% DA +33.3% LA	Pr > F (overall)
Taurine	0.720 ± 0.031	0.430 ± 0.031	0.500 ± 0.031	0.535 ± 0.031	0.0113*
Glycine	4.075 ± 0.290	5.290 ± 0.290	3.410 ± 0.290	3.790 ± 0.290	0.0374*

*Values are LSMean ± SE (pooled). LA = Live instar-1 Artemia; DA = Decapsulated Artemia. Significance codes: * p<0.05; ** p<0.01; *** p<0.001. MP diet was supplied in four particle-size fractions (MP1: 80–100 µm; MP2: 100–150 µm; MP3: 150–240 µm; MP4: 240–450 µm) at equal quantities across all treatments.*

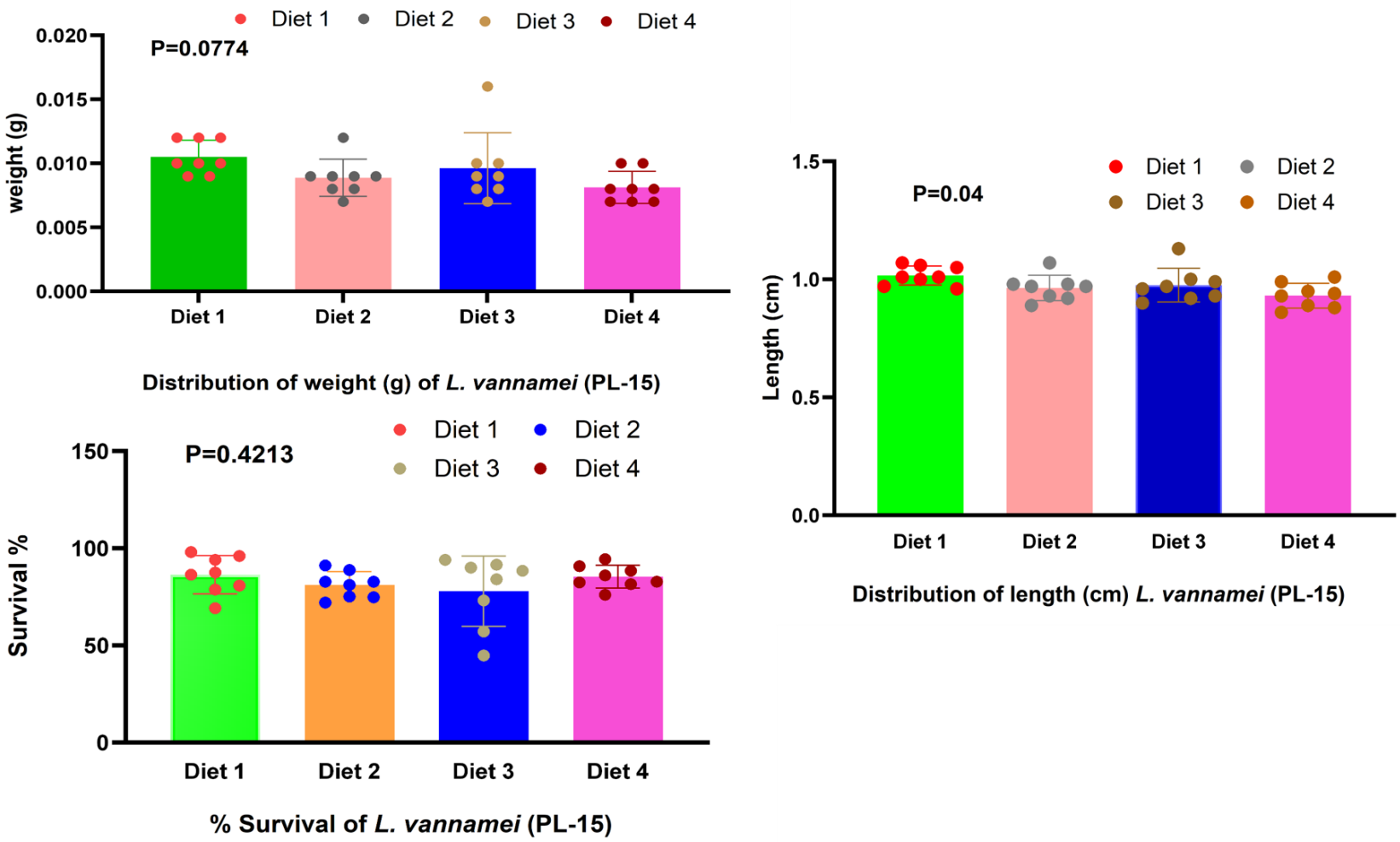


Fig. 1. Distribution of growth performance parameters; length, weight, and survival among *L. vannamei* post-larvae (PL-15) fed four experimental diets (Diet 1 to Diet 4) over the culture period, showing weight distribution (g), length distribution (cm), and percentage survival (%). Data are presented as mean ± SD, with individual data points overlaid on bar graphs.

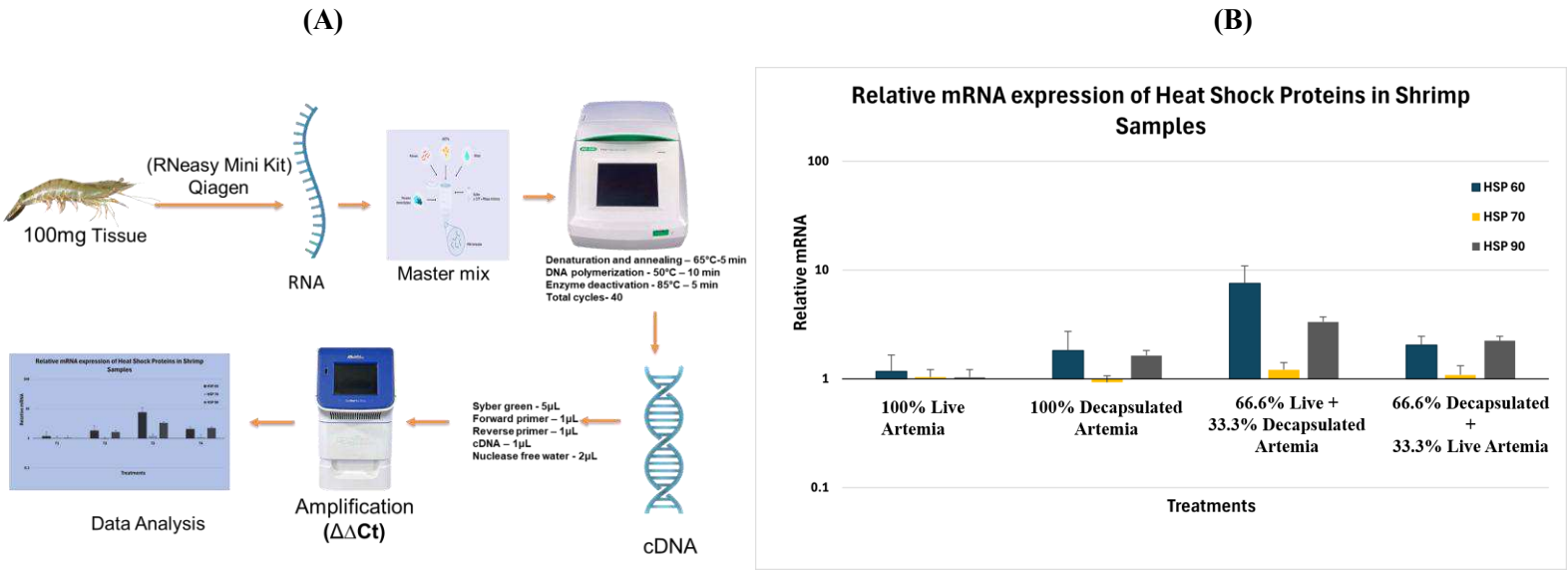


Fig. 2. Gene expression workflow and heat shock protein response in shrimp fed four dietary treatments. (a) Schematic workflow for quantifying heat shock protein (HSP60, HSP70, HSP90) mRNA expression: total RNA was extracted from 100 mg hepatopancreas tissue (RNeasy Mini Kit, Qiagen), reverse-transcribed to cDNA, and amplified by qRT-PCR (SYBR Green, 40 cycles; denaturation/annealing 65 °C–5 min, DNA polymerization 50 °C–10 min, enzyme deactivation 85 °C–5 min) using gene-specific forward/reverse primers. Relative expression was calculated via the ΔΔCt method. (b) Relative mRNA expression of HSP60, HSP70, and HSP90 across the four dietary treatments (100% Live Artemia; 100% Decapsulated Artemia; 66.6% Live + 33.3% Decapsulated; 66.6% Decapsulated + 33.3% Live), shown on a $\log_{10}$ scale. Bars represent mean ± SEM. HSP60 was numerically highest in the 66.6% Live + 33.3% Decapsulated group (5.98-fold vs. control) but did not reach significance ($Pr > F = 0.1448$); HSP90 differed significantly among treatments ($Pr > F = 0.0014$).

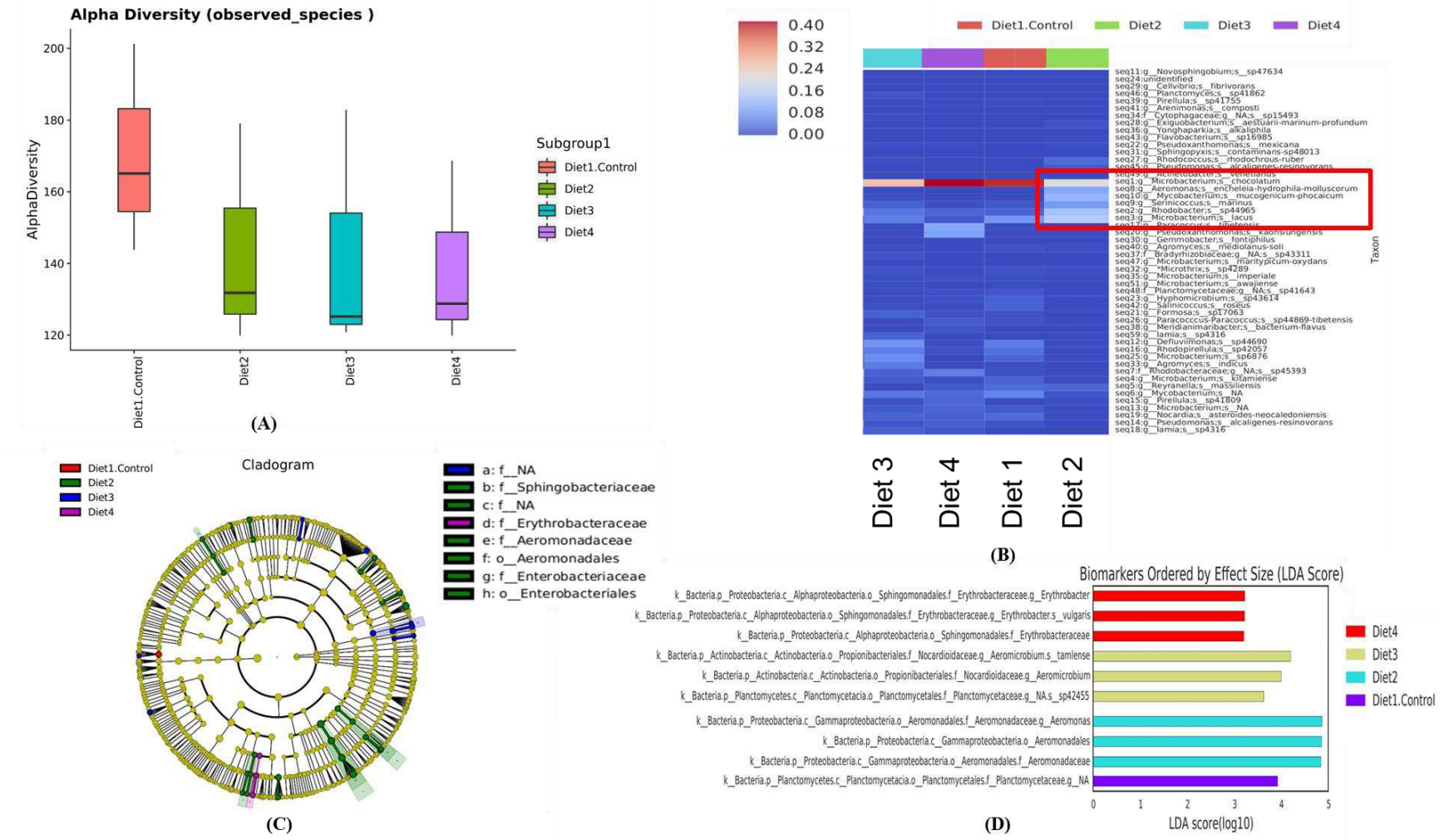


Fig. 3. Gut microbiome of shrimp fed four experimental diets. (A) Alpha diversity (observed species richness); Diet1.Control shows the highest median diversity (~165), vs. ~125–132 for Diets 2–4. (B) Heatmap of relative abundance of the 50 most differentially represented bacterial taxa (SILVA nomenclature); color scale 0.00 (dark blue) to 0.40 (dark red). (C) LEfSe cladogram of taxa differentially abundant by diet, phylum (inner ring) to species (outer ring); colored nodes = significantly enriched taxa per diet, yellow = not significant. (D) LEfSe biomarkers ranked by LDA score ($\log_{10}$); only taxa with LDA≥2.0 and $P<0.05$ (Kruskal-Wallis) shown, colored by enriched diet group.

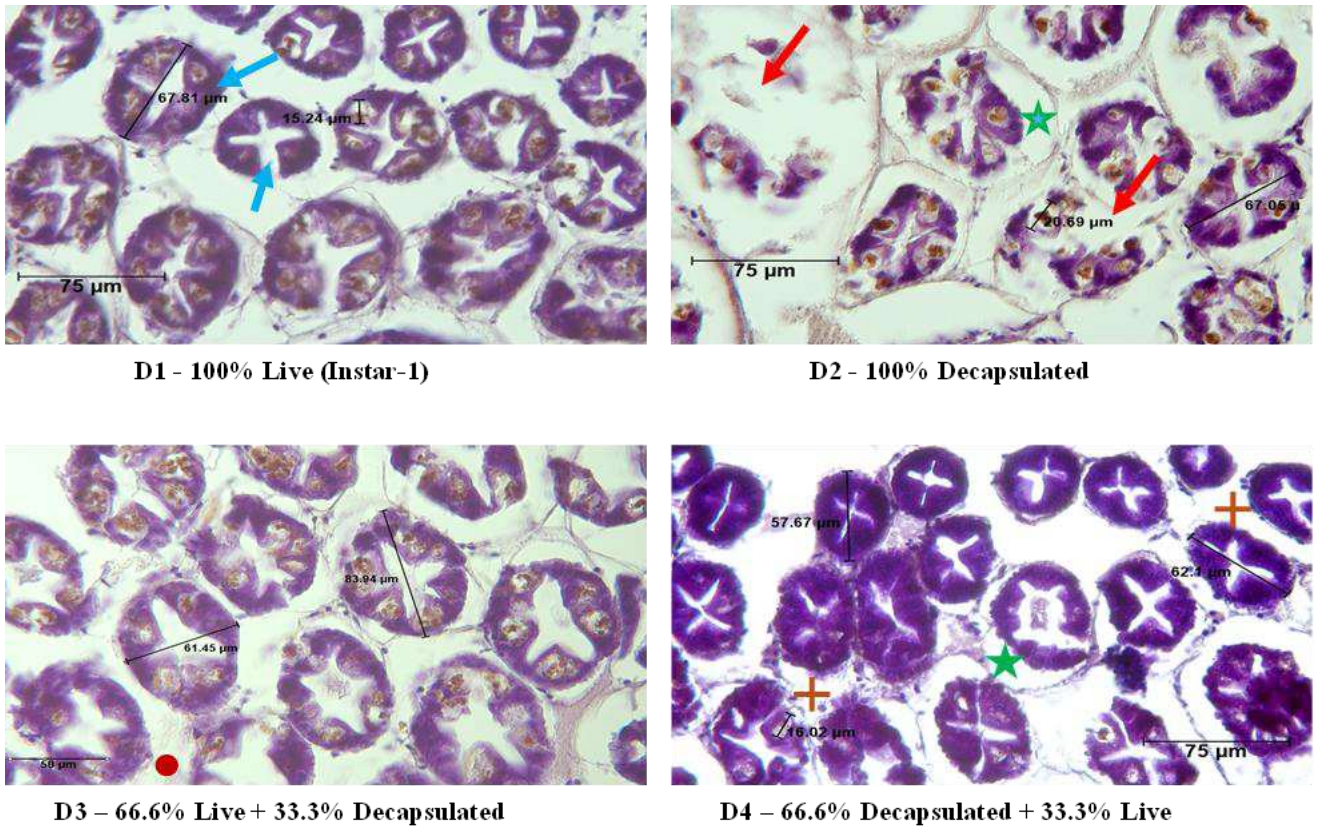


Fig. 4. Photomicrographs of hepatopancreatic tubules (H&E stain) across treatments D1–D4. D1 (100% Live): intact tall columnar epithelium (blue arrows), well-defined luminal border, normal architecture. D2 (100% Decapsulated Artemia): most pronounced epithelial damage (red arrows), cytoplasmic degeneration, epithelial detachment, sloughed cells in lumen (green star). D3 (66.6% live:33.3% decapsulated Artemia): partial epithelial sloughing (red dot), overall continuity retained, less damage than D2. D4 (33.3% live:66.6% Decapsulated Artemia): hyperchromatic/pyknotic nuclei (brown cross), cellular debris (green star), more advanced than D3, less severe than D2. Scale bars = 75 µm (D1,D2,D4) and 50 µm (D3).